This document is confidential and is proprietary to the American Chemical Society and its authors. Do not copy or disclose without written permission. If you have received this item in error, notify the sender and delete all copies.

On the Determination of Halogen Atom Reduction Potentials with Photoredox Catalysts

Journal:	*The Journal of Physical Chemistry*
Manuscript ID	jp-2021-06772d.R3
Manuscript Type:	Article
Date Submitted by the Author:	27-Sep-2021
Complete List of Authors:	Deetz, Alexander; University of North Carolina at Chapel Hill, Chemistry Troian-Gautier, Ludovic; Université Libre de Bruxelles, Chemistry Wehlin, Sara; University of Oxford, Chemistry Piechota, Eric; The Ohio State University, Meyer, Gerald; University of North Carolina at Chapel Hill, Department of Chemistry

SCHOLARONE™
Manuscripts

On the Determination of Halogen Atom Reduction Potentials with Photoredox Catalysts

Alexander M. Deetz, Ludovic Troian-Gautier, Sara A. M. Wehlin, Eric J. Piechota, and Gerald J. Meyer*

Department of Chemistry, University of North Carolina at Chapel Hill, Murray Hall 2202B, Chapel Hill, North Carolina 27599-3290

*Corresponding Author. gjmeyer@email.unc.edu

Abstract. The standard one-electron reduction potentials of halogen atoms, $E°'(X^{\bullet/-})$, and many other radical or unstable species, are not accessible through standard electrochemical methods. Here we report the use of two Ir(III) photoredox catalysts to initiate chloride, bromide, and iodide oxidation in organic solvents. The kinetic rate constants were critically analyzed through a derived diffusional model with Marcus theory to estimate $E°'(X^{\bullet/-})$ in propylene carbonate, acetonitrile, butyronitrile, and dichloromethane. The approximations commonly used to determine diffusional rate constants in water gave rise to serious disagreements with experiment, particularly in high ionic strength dichloromethane solutions, indicating the need to utilize the exact Debye expression. The Fuoss equation was adequate for determining photocatalyst-halide association constants with photocatalysts that possessed +2, +1, and 0 ionic charges. Similarly, the work term contribution in the classical Rehm-Weller expression, necessary for $E°'(X^{\bullet/-})$ determination, accounted remarkably well for the stabilization of the charged reactants as the solution ionic strength was increased. While a sensitivity analysis indicated that the extracted reduction potentials were all within experimental error the same, use of fixed parameters established for aqueous solution provided the periodic trend expected, $E°'(I^{\bullet/-}) < E°'(Br^{\bullet/-}) < E°'(Cl^{\bullet/-})$, in all the organic solvents investigated; however, the potentials were more closely spaced than what would have been predicted based on gas phase electron affinities or aqueous reduction potentials. The origin(s) of such behavior are discussed that provide new directions for future research.

INTRODUCTION

The thermodynamic properties of halogen atoms in fluid solutions are of high relevance to applications in organic, inorganic, and materials chemistry.[1–9] In particular, redox reactions involving halogen atoms are instrumental for C-H bond activation in photoredox catalysis[10,11] and hydrohalic acid splitting for solar energy storage.[12,13] The halogen atom formal reduction potential, $E°(X^{\bullet/-})$, represents a key starting point (Equation 1), yet standard electrochemical techniques do not provide the desired one-electron potentials. Instead, two-electron halide oxidation are observed at metal electrodes with such thermodynamically favored potentials that the one-electron potentials are obscured (Figure S1).[14] Consider for example the case of aqueous iodide oxidation where ~ 800 mV separates the one-electron $E°(I^{\bullet/-})$ = 1.33 V vs NHE from the two-electron $E°(I_3^-/3I^-)$ = 0.54 V vs NHE potential.[9] The formal reduction potentials $E°(X^{\bullet/-})$ found in textbooks are obtained from kinetic measurements or determined indirectly through thermochemical cycles and/or computational methods.[15–20] Experimental measurements require kinetic resolution of atom formation with an electron acceptor, whose $E°'(A^{0/-})$ is known, and a model that relates the kinetic rate constant to the electron transfer driving force, $-\Delta G^o$ (Equation 2).[21] Pulse-radiolysis and stopped-flow techniques have been successfully utilized, however the vast majority of these studies have been restricted to aqueous solutions.[15–20,22] Herein, we extend this kinetic approach to evaluate the use of transition metal photoredox catalysts, PC, with known excited-state reduction potentials $E°'(PC^{*/-})$ to estimate $E°'(X^{\bullet/-})$, where X = Cl, Br, and I, in organic solvents (Equation 3).

$$X^\bullet + e^- \longrightarrow X^- \qquad E°'(X^{\bullet/-}) \tag{1}$$

$$X^- + A \longrightarrow A^{\bullet-} + X^\bullet \qquad -\Delta G° \tag{2}$$

$$X^- + PC^* \longrightarrow PC^- + X^\bullet \qquad -\Delta G° \tag{3}$$

A well-established mechanism for bimolecular redox reactions in fluid solution includes formation of an 'encounter complex' by diffusional encounters of the electron donor and acceptor prior to electron transfer. The remarkable success of the Marcus cross-relation for predicting electron transfer rate constants from known self-exchange rate constants indicates that encounter complex formation can be accounted for, at least for aqueous reactions with small $-\Delta G^o$.[21] Deviations from behavior expected by the Marcus cross-relation are often indicative of alternative inner-sphere mechanisms.[23] Nevertheless, the use of organic solvents and photoredox catalysts

raise new questions that require further analysis and remain largely untested. Since halide oxidation by a photocatalyst excited state occurs in kinetic competition with radiative and non-radiative decay, the electron transfer event must be rapid, often nearing the diffusion limit. The observed kinetics contain information on the electron transfer event, but require corrections for diffusion.[24] As many photocatalysts are cationic and halides are anionic, the charge of the reactants and the ionic strength of the solution must also be accounted for. In principle, Debye-Hückel theory can account for both, yet the utility in low-dielectric solvents deserves further exploration given that many photoredox reactions are studied in organic solutions.

Motivations for this research include a recent review article that summarizes $E°'(X^{\bullet/-})$ values in aqueous and nonaqueous solvents, the latter being largely absent.[9,22] In addition, the well-established and fundamentally sound diffusional model and theoretical framework described herein provide fundamental knowledge that will help identify alternative mechanisms that may (or may not) require as-of-yet undiscovered modifications from which new models can be developed. Finally, kinetic measurements provide the only means that we are aware of that allows halogen atom reduction potentials to be experimentally determined.[12-16] The analysis described herein provides an opportunity to systematically test the assumptions inherent to this approach and is amenable to determination of a wider variety of formal reduction potentials that cannot be obtained through standard electrochemical techniques.

The field of photoredox catalysis has grown dramatically in recent years,[8,25–27] as has the variety of photocatalysts available commercially and through synthetic methods. In this work, we focus on two Ir(III) photocatalysts that are capable of halide oxidation in organic solvents. A measure of the robustness of extracted $E°'(X^{\bullet/-})$ values is their insensitivity to the identity of the photocatalyst utilized to initiate halide oxidation and halogen-atom formation. Careful tuning of the photocatalyst excited-state reduction potential, charge, and molecular structure can provide insights into which assumptions are most valid and which are not. Some alternative $(d\pi)^6$ transition metal photocatalysts are reported herein with this goal in mind. Indeed, a wider variety of photocatalysts would certainly provide more reliable estimates of $E°'(X^{\bullet/-})$ and provide directions for future research.

EXPERIMENTAL

Materials. *n*-Butyronitrile (BuCN, Acros Organics, 99 %), acetonitrile (Acros, 99.9%, Anhydrous), propylene carbonate (Acros, 99.8% Anhydrous) and dichloromethane (Acros, 99.8% Anhydrous) were used as received. Argon gas (Airgas, 99.998 %) was passed through a Drierite drying tube before use. Tetrabutylammonium iodide (TBAI, Sigma-Aldrich, ≥ 99.0 %), tetrabutylammonium bromide (TBABr, Sigma-Aldrich, ≥ 99.0 %), and tetrabutylammonium chloride (TBACl, Sigma-Aldrich, ≥ 99.0 %) were recrystallized from acetone and diethyl ether and stored in a vacuum desiccator. Tetrabutylammonium hexafluorophosphate ($TBAPF_6$, Sigma-Aldrich, for electrochemical analysis, ≥ 99.9 %), lithium perchlorate ($LiClO_4$, Sigma-Aldrich, for electrochemical analysis, ≥ 99.9 %), lithium iodide (Sigma-Aldrich), lithium bromide (Sigma-Aldrich), and tri-*p*-tolylamine (TCI America, ≥ 98 %) were stored in a vacuum desiccator and used as received.

Electrochemistry. Solutions were prepared with 0.1 M supporting electrolyte and sparged with argon for 30 minutes before electrochemical experiments. $TBAPF_6$ was used as the supporting electrolyte for organic solvents and $LiClO_4$ in water. Measurements were performed with a BASi Epsilon potentiostat in a standard three electrode cell with a platinum disk working electrode, platinum mesh counter electrode, and Ag/Ag^+ pseudo reference that was externally referenced to ferrocene for organic solvents or SCE for water.

Sample Preparation for Photophysical and Photochemical Measurements. Samples were prepared in an argon glovebox using solvents that were previously deaerated by purging with argon for 45 minutes. Stock solutions of photocatalysts were prepared by dissolving the desired complex in ~20 mL of solvent such that the solution had an absorbance value near 0.1 at the excitation wavelength (~50 μM). A 3 mL aliquot of the iridium solution was transferred into a custom-made photometric quartz cuvette and sealed with a septum while in the glovebox Tetrabutylammonium halide or lithium halide salts were dissolved in 2 mL of the iridium stock solution (~20 mM halide concentration) and sealed with a septum while in the glovebox. Experiments performed at fixed ionic strengths were setup in an identical fashion with the exception of electrolyte added to the solutions. Similar sample preparation was used for transient absorption experiments with the exception that the concentration was adjusted to reach an absorbance value between 0.4 and 0.8 at 420 nm.

Transient Absorption. Nanosecond transient absorption measurements were acquired on a previously described apparatus.[28] Briefly, a Q-switched, pulsed Nd:YAG laser (Quantel U.S.A. (BigSky) Brilliant B 5-6 ns full width at half-maximum (fwhm), 1 Hz, ~10 mm in diameter) was utilized. The 355 nm laser was passed through an OPO and tuned to 420 nm. The laser irradiance at the sample was attenuated to 1.5-3 mJ/pulse. The probe lamp consisted of a 150 W xenon arc lamp that was pulsed at 1 Hz. Signal detection was achieved using a monochromator (SPEX 1702/04) optically coupled to an R928 photomultiplier tube (Hamamatsu) at a right angle to the excitation laser. Transient data were acquired with a computer-interfaced digital oscilloscope (LeCroy 9450, Dual 330 MHz) with an overall instrument response time of ~10 ns. An average of 30 laser pulses were collected at each wavelength of interest over the 400-800 nm range. Intervals of 10 nm were used between 400 and 600 nm while intervals ranging from 10 to 40 nm were used between 600 and 800 nm.

UV−Vis Absorption. UV−vis absorption spectra were recorded on a Varian Cary 60 UV−vis spectrophotometer with a resolution of 1 nm.

Steady-State Photoluminescence. Steady-state PL spectra were recorded on a Horiba Fluorolog 3 fluorimeter and corrected by calibration with a standard tungsten-halogen lamp. Samples were excited at 420 nm. The intensity was integrated for 0.1 s at 1 nm resolution and averaged over 3 scans.

Time-Resolved Photoluminescence. Time-resolved PL data were acquired on a nitrogen dye laser with excitation centered at 445 nm. Pulsed light excitation was achieved with a Photon Technology International (PTI) GL-301 dye laser that was pumped by a PTI GL-3300 nitrogen laser. The PL was detected by a Hamamatsu R928 PMT optically coupled to a ScienceTech Model 9010 monochromator terminated into a LeCroy Waverunner LT322 oscilloscope. Decays were monitored at the PL maximum and averaged over 180 scans.

Extinction Coefficient of Reduced Photocatalyst. The absorption spectrum of the singly reduced Iridium complex was determined using a procedure adapted from literature.[29] A 10 μM solution of **Ir** with 10 mM tri-*p*-tolylamine (Me-TPA) was irradiated with 420 nm light (1.5 mJ/cm^2). Laser excitation of **Ir** resulted in electron transfer from the TPA to **Ir***. Transient absorption spectra were recorded, normalized at the TPA$^+$ maxima, and the normalized spectrum of the oxidized TPA was subtracted to give the difference spectrum between the reduced **Ir** and

the ground state. The concentration of reduced complex formed was calculated from the known extinction coefficient of the oxidized TPA.[30]

Stern-Volmer Experiments. An iridium solution with an absorbance of 0.1 at 420 nm was prepared in the argon-purged solvent of choice. Various quencher solutions with known concentrations were prepared in each solvent. The desired quencher was incrementally added to a solution of iridium photosensitizer and the excited-state quenching was monitored by steady-state and time-resolved photoluminescence. The decrease of excited-state lifetime and photoluminescence were directly related to the concentration of quencher. The corresponding Stern-Volmer plot can be obtained using the following equation:

$$\frac{\sum(PLI_0)}{\sum(PLI)} = \frac{\tau_0}{\tau} = 1 + K_{SV}[Q] = 1 + k_q\tau_0[Q]$$

For Ir-5,5'-CF_3 in dichloromethane, a combination of static and dynamic excited-state quenching occurred. Upward curvature of the photoluminescence integral (PLI_0/PLI) ratio was observed. The combination of these two processes was analyzed through a combined Stern-Volmer analysis that has a quadratic dependence on the concentration of the quencher:

$$\frac{\sum(PLI_0)}{\sum(PLI)} = 1 + (K_D + K_S)[Q] + K_D K_S[Q]^2$$

RESULTS AND DISCUSSION

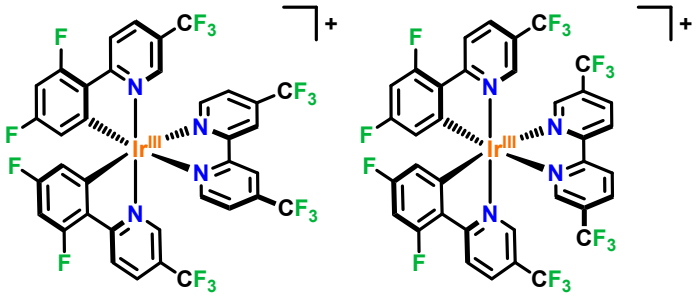

Figure 1. $[Ir(dF\text{-}CF_3ppy)_2(4,4'\text{-}(CF_3)_2bpy)]^+$, (Ir-4,4'-$CF_3$), and $[Ir(dF\text{-}CF_3ppy)_2(5,5'\text{-}(CF_3)_2bpy)]^+$, (Ir-5,5'-$CF_3$), were isolated as PF_6^- or Cl^- salts for experiments in organic solvents or water, respectively.

(1) Excited State Quenching. The iridium photocatalysts, abbreviated Ir-4,4'-CF_3 and Ir-5,5'-CF_3 (Figure 1), exhibited spectroscopic properties typical of charge-transfer excited states[31]

with intense room temperature photoluminescence (PL) centered around 600 nm (Figure 2). These photocatalysts are commercially available members of a larger family of well characterized $(d\pi)^6$ inorganic transition metal complexes. The room temperature data reported here is fully consistent with expectations of PL from a single thermally equilibrated excited state that undergoes diffusional electron transfer in agreement with Kasha's rule. The absorption and PL spectra displayed small, yet measurable, solvatochromism in propylene carbonate, acetonitrile, butyronitrile, dichloromethane, and water. Pulsed-light excitation yielded PL decays that were well described by a first-order kinetic model with excited state lifetimes, τ_o, that were more sensitive to the solvent identity than were the absorption or PL spectra, Table 1. The iridium photocatalysts displayed quasi-reversible $E°'(Ir^{+/0})$ reductions with similar potentials in the four organic solvents (Table 1, Figure S2). Excited-state reduction potentials were determined from $E°'(Ir^{+*/0}) = E°'(Ir^{+/0}) - \Delta G_{es}$, where ΔG_{es} is the Gibbs free energy stored in the excited state.[32,33]

Table 1. Solvent dependent excited-state lifetimes (τ_o), ground-state reduction potentials ($E°'(Ir^{+/0})$), and excited-state reduction potentials ($E°'(Ir^{*+/0})$) of the iridium photocatalysts.

Solvent	τ_o (ns) Ir-4,4'-CF_3	$E°'(Ir^{+/0})$[a] Ir-4,4'-CF_3	$E°'(Ir^{+*/0})$[a,b] Ir-4,4'-CF_3
Water	115	−0.61[c]	1.80[c]
Propylene Carbonate	345	−1.25	1.24
Acetonitrile	428	−1.24	1.19
Butyronitrile	487	−1.22	1.23
Dichloromethane	770	−1.16	1.27

Solvent	τ_o (ns) Ir-5,5'-CF_3	$E°'(Ir^{+/0})$[a] Ir-5,5'-CF_3	$E°'(Ir^{+*/0})$[a,b] Ir-5,5'-CF_3
Propylene Carbonate	63	−1.11	1.28
Acetonitrile	83	−1.15	1.21
Butyronitrile	96	−1.12	1.25
Dichloromethane	286	−1.08	1.29

[a]V vs $Fc^{+/0}$ unless otherwise specified. [b]Estimated by $E°'(Ir^{+*/0}) = E°'(Ir^{+/0}) - \Delta G_{es}$. [c]V vs NHE.

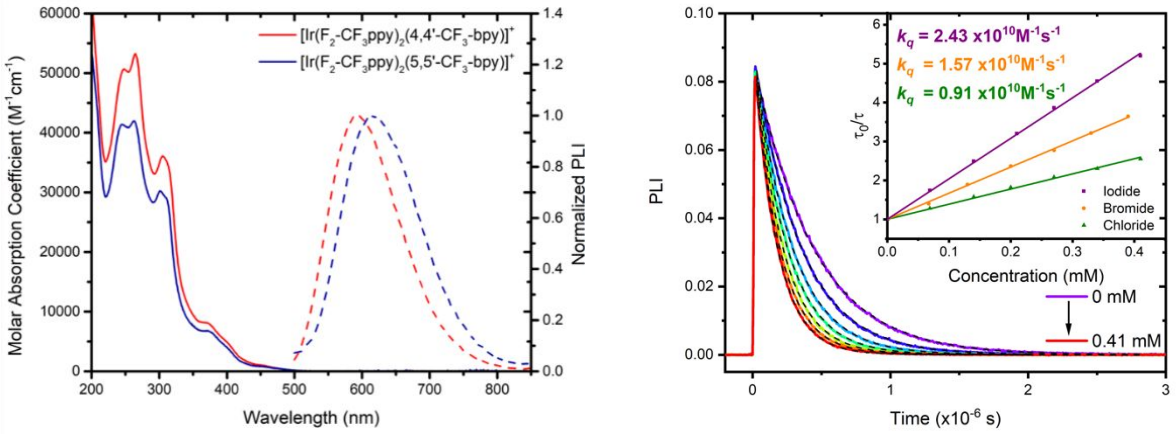

Figure 2. Absorbance and steady-state photoluminescence data for the corresponding photocatalyst in acetonitrile (left), and time-resolved PL of Ir-4,4'-CF_3 with increasing amounts of chloride in argon-purged acetonitrile at room temperature. The inset provides Stern-Volmer plots for iodide, bromide, and chloride (right).

Chloride, bromide, and iodide ions quenched the steady-state PL intensity and the excited-state lifetime of both iridium photocatalysts in all four organic solvents (Figure S3-S10). Importantly, there was no evidence for ligand-loss or other permanent photochemistry in any experiment reported herein.[34–36] Representative quenching data in acetonitrile is shown in Figure 2. Stern-Volmer plots of τ_o/τ were indicative of dynamic quenching under all conditions except in dichloromethane, which showed evidence for an additional static quenching pathway manifest as a significant decrease in the initial PL amplitude (Figure S10) that is absent in Figure 2a. In contrast, within experimental error the initial amplitudes of the time-resolved PL decays were independent of the halide concentration in the other organic solvents investigated. Second-order quenching rate constants, k_q, were extracted from Stern-Volmer analysis and ranged from 0.52 x10^9 $M^{-1}s^{-1}$ to 32.2 x10^9 $M^{-1}s^{-1}$ depending on the solvent (propylene carbonate, acetonitrile, butyronitrile, and dichloromethane) and halide ion. In aqueous solutions, quenching was observed with iodide and bromide; chloride concentrations up to 100 mM did not impact excited-state relaxation (Figure S11).

Table 2. Second-order quenching rate constants for both photocatalysts extracted from Stern-Volmer analysis.

Solvent	k_q I[a] Ir-4,4'-CF_3	k_q Br[a] Ir-4,4'-CF_3	k_q Cl[a] Ir-4,4'-CF_3
Water	10.6	0.00639	--
Propylene Carbonate	3.41	1.82	0.52
Acetonitrile	24.3	15.7	9.09
Butyronitrile	21.0	16.0	14.4
Dichloromethane	26.1	20.4	16.7

Solvent	k_q I[a] Ir-5,5'-CF_3	k_q Br[a] Ir-5,5'-CF_3	k_q Cl[a] Ir-5,5'-CF_3
Propylene Carbonate	4.04	1.72	0.53
Acetonitrile	29.9	14.6	8.39
Butyronitrile	28.0	19.0	14.1
Dichloromethane	32.2	25.9	23.3

[a] $x10^9$ $M^{-1}s^{-1}$

Nanosecond transient absorption spectroscopy provided evidence for a reductive quenching mechanism by bromide and iodide where features characteristic of the oxidized halide and reduced iridium catalyst were evident (Figure 3).[37] It has been well established that the primary halogen photoproduct, $X^{\bullet}$ (where X = Br or I), rapidly reacts with excess X^- to form $X_2^{\bullet -}$.[16,38] The absorption band centered near 520 nm is assigned to the reduced Ir catalyst and the broad absorption in the red region as well as the absorption onset in the blue region are assigned to $X_2^{\bullet -}$. The transient spectra, simulated by standard addition of the known spectra of the reduced catalyst and $X_2^{\bullet -}$ are overlaid on the spectral data as solid lines. Excited-state electron transfer from chloride was evident only as a small amplitude feature attributed to the reduced catalysts without detection of the oxidized chloride product(s) (Figure S12).

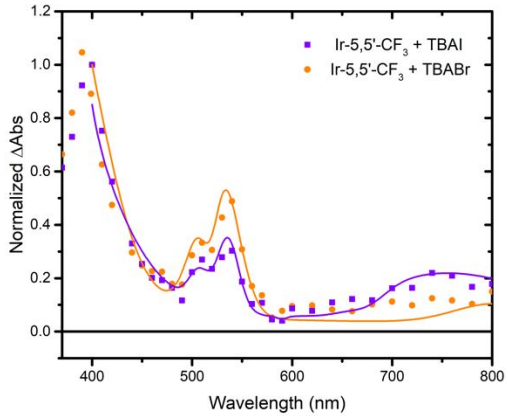

Figure 3. Transient absorption spectra recorded at 1 μs time delay following pulsed 420 nm light excitation of a solution containing 250 μM Ir-5,5-CF_3 and 4 mM TBAX (X = Br or I) in argon-purged CH_2Cl_2. The solid lines are simulated spectra of equimolar concentrations of reduced $[Ir\text{-}5,5'\text{-}CF3]^0$ and $X_2^{\bullet -}$.

A brief overview of the approach used to extract $E°'(X^{\bullet/-})$ is described in order to introduce the halogen reduction potentials, tabulated in Table 3, which are intended to be a starting place for comparison in future studies. We urge caution in the use of these potentials outside of this context. Nevertheless, we strongly encourage others to critically examine the values reported herein to help refine our knowledge of the redox properties of halogen atoms and other unstable radical species that are critically important to photocatalysis and energy applications.

Electron transfer rate constants, k_{et}, were extracted from the measured k_q with a diffusional model that requires a steady-state approximation and knowledge of bimolecular diffusional rate constants and association constants. The k_{et} was then used to determine the driving force, $-\Delta G^o$, for electron transfer through Marcus theory. Within the Marcus expression, determination of the driving force for electron transfer from k_{et} requires knowledge of the reorganization energy, λ, and the electronic coupling matrix element, H_{AB}, which is incorporated into the pre-exponential factor, A, in the simplified expression (Equation 4).[21] Typical values of λ = 1 eV and $A = 10^{11}$ s^{-1} were assumed unless otherwise specified. The $-\Delta G^o$ was then used in conjunction with $E°'(Ir^{+*/0})$ to estimate the halogen atom reduction potentials through the Rehm-Weller equation (Equation 5), where G_w is the work required to bring the photoexcited catalyst and halide together in a so-called 'encounter complex'.[39,40] The work term is small in polar solvents but becomes significant in nonpolar solvents and/or with highly charged reactants.

$$k_{et} = \frac{2\pi}{\hbar}|H_{AB}|^2 \frac{1}{\sqrt{4\pi\lambda k_b T}} \exp\left(-\frac{(\lambda + \Delta G^o)^2}{4\lambda k_b T}\right) = A \exp\left(-\frac{(\lambda + \Delta G^o)^2}{4\lambda k_b T}\right) \quad (4)$$

$$\Delta G^o = \left\{\left[E^{o\prime}(X^{\bullet/-}) - E^{o\prime}(Ir^{+*/0})\right] - G_w\right\} \quad (5)$$

Table 3. Estimated formal reduction potentials of iodide, bromide, and chloride in the indicated solvents.[a]

Solvent	$E°'(I^{\bullet/-})$[b]	$E°'(Br^{\bullet/-})$[b]	$E°'(Cl^{\bullet/-})$[b]
Water	1.27 ± 0.46[c]	1.84 ± 0.26[c]	--
Prop. Carb.	0.85 ± 0.36	0.96 ± 0.34	1.06 ± 0.32
Acetonitrile	0.68 ± 0.38	0.77 ± 0.36	0.83 ± 0.35
Butyronitrile	0.80 ± 0.36	0.84 ± 0.35	0.86 ± 0.35
Dichloromethane	1.00 ± 0.30	1.02 ± 0.30	1.04 ± 0.29

[a]The potentials are averaged values estimated through kinetic measurements of Ir-4,4'-CF_3 and Ir-5,5'-CF_3 that rely on key assumptions (see text) and thus should be considered carefully. Sensitivity analysis was performed on key assumptions, which is reflected by the designated uncertainty. [b]V vs $Fc^{+/0}$ unless otherwise specified. [c]V vs NHE estimated from kinetic measurement with Ir-4,4'-CF_3.

A sensitivity analysis was performed to estimate the uncertainty in the extracted reduction potentials given in Table 3 stemming from assumptions and approximations necessary in the kinetic analysis. The value for parameters that were identified as the most likely sources of uncertainty were varied one at a time over physically realistic ranges to determine their influence on the reduction potential for each halide in each solvent (*vide infra*, Section 8). Despite the magnitude of uncertainty stemming from parameters within the model, the estimated reduction potentials are reported to two decimal places to reflect the precision of the experimentally measured quenching rate constants. For instance, quenching rate constants for Ir-4,4'-CF_3 in dichloromethane of 2.61×10^{10} M^{-1} s^{-1} and 1.67×10^{10} M^{-1} s^{-1} for iodide and chloride, respectively, are reproducible and reflect a measurable difference in rate constants for halide oxidation. Below, the details of the analysis are given with the introduction of additional experiments designed to test the validity of the key assumptions made.

(2) Diffusional Electron Transfer Mechanism. The kinetic data indicate a diffusional electron transfer quenching mechanism wherein the excited state and the halide diffuse together to form an encounter complex, *EC*, prior to electron transfer (Scheme 1), with the overall rate law in Equation 6:

$$\frac{d[P]}{dt} = k_q[Ir^{+*}][X^-] \quad (6)$$

where $[P]$ is the product pair after the moment of electron transfer in the composite mechanism. Within the encounter complex, electron transfer occurs by a first-order reaction (Equation 7).

$$\frac{d[P]}{dt} = k_{et}[EC] \quad (7)$$

Scheme 1. Composite mechanism for diffusional electron transfer

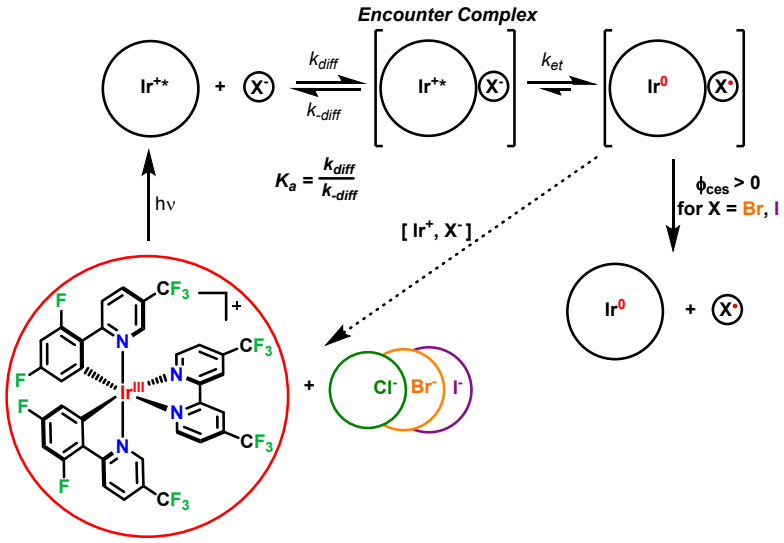

Rate constants for electron transfer, k_{et}, have typically been extracted from k_q by application of a steady-state approximation. The *EC* concentration is assumed to be constant and negligibly small throughout the kinetic measurement:

$$0 \cong \frac{d[EC]}{dt} = k_{diff}[Ir^{+*}][X^-] - k_{-diff}[EC] - k_{et}[EC] \quad (8)$$

$$[EC] = \frac{k_{diff}[Ir^{+*}][X^-]}{k_{-diff} + k_{et}} \quad (9)$$

Substitution of Equation 9 into Equation 7 yields:

$$\frac{d[P]}{dt} = k_{et}\left(\frac{k_{diff}[Ir^{+*}][X^-]}{k_{-diff} + k_{et}}\right) \quad (10)$$

And by inspection of Equation 10 and Equation 6:

$$k_q = \frac{k_{et}k_{diff}}{k_{-diff} + k_{et}} \quad (11)$$

Which is conveniently rewritten as:

$$\frac{1}{k_q} = \frac{1}{k_{diff}} + \frac{1}{K_a k_{et}} \quad (12)$$

$$K_a = \frac{k_{diff}}{k_{-diff}} \quad (13)$$

Thus, determination of k_{et} requires knowledge of the diffusional rate constant, k_{diff}, and the association constant for *EC* formation, K_a. The opposite charges of the halides and photocatalysts described herein led to favorable K_a values and enhanced diffusional rate constants. These

parameters are crucial to extracting k_{et} and the following sections explicitly evaluate methods for estimating k_{diff} and K_a from a theoretical and experimental perspective.

(3) Diffusional Rate Constants. Assuming molecules of spherical symmetry, bimolecular diffusional rate constants have been estimated by Equation 14[41]:

$$k_{diff} = 4\pi N_A(D_a + D_b)\beta \quad (14)$$

where N_A is Avogadro's number, D_a and D_b are the diffusion coefficients of the reactants and β is the reaction radius. Diffusion coefficients may be measured experimentally or estimated through the Stokes-Einstein relationship (Equation 15), where k_B is the Boltzmann constant, T is temperature, η is the solvent viscosity, and r_i is the reactant radius where I^- = 2.06 Å, Br^- = 1.96 Å, Cl^- = 1.84 Å,[42] and the radii of the Ir complexes were estimated as 6.8 Å by DFT.

$$D_i = \frac{k_B T}{6\pi r_i \eta} \quad (15)$$

The reaction radius for neutral molecules is usually taken to be the sum of reactant radii, denoted R. When the reactants are charged, β represents an *effective* reaction radius that is related to the potential energy, $U(r)$, of the two separated ions in solution integrated over distance from the sum of the reactant Van der Waals radii, R, to infinity:

$$\beta^{-1} = \int_R^\infty \frac{exp\left(\frac{U(r)}{k_B T}\right)}{r^2} dr \quad (16)$$

The simplest expression for potential energy, also referred to as the work term, is a Coulomb's law-type expression, shown in Equation 17, where z_i is the charge of the reactant, e is the elementary charge of an electron, ε_r is the solvent dielectric constant, and ε_0 is vacuum permittivity:

$$U(r) = \frac{z_a z_b e^2}{4\pi\varepsilon_r\varepsilon_0 r} \quad (17)$$

While commonly used and recommended by IUPAC for calculating work terms in photochemistry,[43] it is prudent to note that Equation 17 holds only at infinite dilution *without* consideration of screening due to other ions. Nevertheless, this expression is convenient and useful for analytical evaluation of the integral such that:

$$\beta = \frac{z_a z_b r_0}{exp\left(\frac{z_a z_b r_0}{R}\right) - 1} \quad (18)$$

where $r_0 = e^2/(4\pi\varepsilon_r\varepsilon_0 k_b T)$. To account for ion screening, an additional term is often included for the attenuated potential in an ionic atmosphere (Equation 19) where κ^{-1} is the Debye length (Equation 20) and μ is the solution ionic strength[44–48]:

$$U(r) = \frac{z_a z_b e^2}{4\pi\varepsilon_r\varepsilon_0 r} - \frac{z_a z_b e^2}{4\pi\varepsilon_r\varepsilon_0}\kappa \quad (19)$$

$$\kappa^{-1} = \sqrt{\frac{\varepsilon_r\varepsilon_0 k_B T}{2000 e^2 N_A \mu}} \quad (20)$$

Integration of Equation 16 using the modified expression for potential energy has been used to obtain a 'corrected' effective reaction radius and by extension, a corrected diffusional rate constant conveniently written as Equations 21 and 22, respectively, where β^0 and k_{diff}^0 are those calculated at infinite dilution:

$$\beta = \beta^0 exp(z_a z_b r_0 \kappa) \quad (21)$$

$$k_{diff} = k_{diff}^0 exp(z_a z_b r_0 \kappa) \quad (22)$$

While this approach has been utilized successfully,[38,41,49–52] note that Equations 17 and 19 are varying degrees of approximations of the 'exact' potential energy expression from Debye in Equation 23[24,47,53]:

$$U(r) = \frac{z_a z_b e^2}{4\pi\varepsilon_r\varepsilon_0 r}\left(\frac{1}{2}\left(\frac{exp(\kappa\sigma_a)}{1+\kappa\sigma_a} + \frac{exp(\kappa\sigma_b)}{1+\kappa\sigma_b}\right)exp(-\kappa r)\right) \quad (23)$$

where σ is the radius of the reactant plus the radius of the main counterion in the ion's atmosphere. However, a limitation of the full expression is that substitution into Equation 16 gives rise to a double exponential in the integrand that requires numerical integration. A thorough comparison of these methods for estimating diffusional rate constants has been previously described by Chiorboli *et al.* in aqueous solutions.[24] Here we demonstrate the often overlooked and sometimes profound shortcomings of using approximate formulations for potential energy within the Debye-Hückel framework to estimate bimolecular diffusion in *nonaqueous* electrolyte solutions.

In nonpolar solvents such as dichloromethane, electrolyte concentration has been shown to have a dramatic effect on measured reduction potentials.[54,55] Thus, in our effort to estimate halogen reductions under conditions similar to those where halogen atoms may be generated in photoredox catalysis,[7,56] quenching rate constants reported in Table 2 were determined from experiments performed in the absence of an added electrolyte. When charged photocatalysts and halides are used in the absence of a supporting electrolyte, substantial changes to the ionic strength, and therefore the diffusional rate constant, occur throughout the titration. Therefore, Stern-Volmer-

type titrations are commonly performed in the presence of an inert supporting electrolyte that maintains a nearly constant ionic strength throughout the experiment. On the other hand, expressions to determine k_{diff} within the Debye-Hückel framework were derived with the assumption of very dilute ionic solutions with deviations expected even at modest ionic strengths (ca. 10^{-4} M).[41]

Thus, we sought to compare the experimentally measured quenching rate constants, the calculated diffusional rate constants (using the potential energy expressions from Equation 19 or 23), and the extracted electron transfer rate constants from experiments performed with and without a 0.1 M $TBAPF_6$ supporting electrolyte in both dichloromethane and acetonitrile. The data for Ir-4,4'-CF_3 are tabulated in Table 4. An average ionic strength of 0.2 mM was assumed for experiments without supporting electrolyte.

Table 4. Quenching rate constants measured with and without[a] a 0.1 M $TBAPF_6$ electrolyte and the corresponding k_{et} and k_{diff} values calculated from the method stated.

	k_q[b] (M^{-1} s^{-1})	k_{diff} (approx.)[c] (M^{-1} s^{-1})	k_{et} (approx.)[c] (s^{-1})	k_{diff} (exact)[d] (M^{-1} s^{-1})	k_{et} (exact)[d] (s^{-1})
			CH_2Cl_2		
Cl^-	1.67×10^{10}	5.45×10^{10}	2.24×10^{7}	8.08×10^{10}	1.96×10^{7}
Br^-	2.04×10^{10}	5.19×10^{10}	3.31×10^{7}	7.69×10^{10}	2.73×10^{7}
I^-	2.61×10^{10}	5.00×10^{10}	5.63×10^{7}	7.41×10^{10}	4.15×10^{7}
			CH_2Cl_2 + 0.1 M $TBAPF_6$ electrolyte		
Cl^-	2.05×10^{9}	508	–42.9	2.33×10^{10}	1.90×10^{8}
Br^-	3.44×10^{9}	483	–41.1	2.23×10^{10}	3.46×10^{8}
I^-	6.28×10^{9}	465	–39.7	2.16×10^{10}	7.55×10^{8}
			CH_3CN		
Cl^-	9.09×10^{9}	5.14×10^{10}	1.27×10^{9}	5.23×10^{10}	1.27×10^{9}
Br^-	1.57×10^{10}	4.91×10^{10}	2.62×10^{9}	5.00×10^{10}	2.59×10^{9}
I^-	2.43×10^{10}	4.75×10^{10}	5.56×10^{9}	4.84×10^{10}	5.46×10^{9}
			CH_3CN + 0.1 M $TBAPF_6$ electrolyte		
Cl^-	2.45×10^{9}	5.55×10^{9}	1.25×10^{9}	3.20×10^{10}	7.59×10^{8}
Br^-	5.42×10^{9}	5.31×10^{9}	-7.30×10^{10}	3.07×10^{10}	1.84×10^{9}
I^-	9.10×10^{9}	5.13×10^{9}	-3.21×10^{9}	2.98×10^{10}	3.58×10^{9}

[a]A 0.2 mM average ionic strength was assumed in calculations. [b]Experimentally measured. [c]The diffusional rate constants calculated with the approximation given in Equation 19 and the corresponding electron transfer rate constants, k_{et}. Note that the negative rate constants in 0.1 M electrolyte are reported to demonstrate the inadequacy of this level of theory. [d]The diffusional rate constants calculated with the exact expression given in Equation 23 and the corresponding electron transfer rate constants, k_{et}.

In the presence of a 0.1 M supporting electrolyte, the measured k_q values were attenuated by a factor of 2 to 4 in acetonitrile and 4 to 8 in dichloromethane relative to those measured in neat solvent (Figure S13 and S14). Because the opposite charges of the photocatalysts and halides lead to enhanced bimolecular diffusional rate constants, screening of this attractive force by a

supporting electrolyte was anticipated to yield a smaller k_q. Indeed, the presence of electrolyte had the greatest impact with chloride and the smallest with iodide, consistent with the expectation that charge screening has a greater effect with a higher charge-to-size ratio anion.

Diffusional rate constants were determined using Equation 14, Equation 16, and either potential energy Equation 19 or 23. When no external electrolyte was present, the use of either potential energy expression yielded qualitatively 'realistic' values of k_{diff}. In the context of this discussion, a 'realistic' k_{diff} refers to a value larger than that for uncharged species *i.e.* where $\beta = R$, since k_{diff} for charged species should asymptotically approach the value for neutral molecules with increasing ionic strength.[24] The k_{diff} for neutral species of the same size as iodide and the iridium photocatalyst are 1.67×10^{10} and 2.51×10^{10} M^{-1} s^{-1} in dichloromethane and acetonitrile, respectively. In acetonitrile, the two diffusional models were in good agreement with less than 4% discrepancy. However, in dichloromethane the approximate expression underestimated the exact expression by nearly a factor of 2. The impact of such discrepancy on k_{et} is amplified as k_q approaches the diffusional limit.

When 0.1 M $TBAPF_6$ was present, diffusional rate constants calculated using the approximate potential energy expression led to unrealistic values of k_{diff}. Not only were these calculated k_{diff} smaller than what would be anticipated for neutral species (*vide supra*), the measured k_q values were larger than the estimated k_{diff} for all experiments except chloride in acetonitrile. Moreover, it is noteworthy that these shortcomings are exacerbated in lower dielectric solvents and/or at higher ionic strengths where physically meaningless negative electron transfer rate constants were extracted. Thus, tremendous caution is advised when using approximate expressions (Equation 19) and should be avoided altogether in lower dielectric solvents and/or at higher ionic strengths. Subsequent discussion will rely on diffusional rate constants obtained exclusively from Equation 23.

(4) Ionic Strength Effects on Electron Transfer Rate Constants. Correction for diffusion enabled comparison of the intrinsic electron transfer rate constants with and without added electrolyte (Note that k_{et} values were determined using values for K_a that are discussed in the subsequent section.) In dichloromethane, extracted k_{et} values measured without electrolyte were approximately an order of magnitude smaller than in the presence of 0.1 M $TBAPF_6$. This attenuation of k_{et} implied that the oxidation of halides was more thermodynamically favored in the presence of a supporting electrolyte. This behavior is consistent with a smaller work term in the

Rehm-Weller expression (Equation 5) for associating charged species at higher ionic strength; indeed, halogen reduction potentials extracted from experiments with and without electrolyte are in remarkably close agreement when this necessary correction is included (*vide infra*, Section 7).

The impact of ionic strength is greatly diminished in the more polar CH_3CN.[54] Indeed, k_{et} values measured with and without electrolyte varied by less than a factor of two, with larger values measured in neat acetonitrile. The slightly larger k_{et} in the absence of electrolyte may be due to a smaller reorganization energy, λ, for a process with the same driving force, and thus, estimated halogen reduction potential. Dielectric continuum theory predicts an increase in λ with a larger static dielectric constant, ε_r, which is a consequence of adding an electrolyte to a solvent. Alternatively, the larger k_{et} may result from the assumptions made in estimating k_{diff} and/or K_a. The assumptions inherent to K_a estimations are discussed and probed experimentally in the next section.

Table 5. Encounter complex association equilibrium constants for Ir-4,4'-CF_3 or Ir-5,5'-CF_3 with halides in the indicated solvents.[a]

Solvent	K_a Cl (M^{-1})	K_a Br (M^{-1})	K_a I (M^{-1})
Water	--	3.67	3.81
Propylene Carbonate	4.17	4.28	4.39
Acetonitrile	8.67	8.82	8.95
Butyronitrile	18.7	18.8	18.9
Dichloromethane	1075	1016	971

[a]Values were obtained using Equations 24 and 25 using a photocatalyst radius of 6.8 Å.

(5) Association Constant for Encounter Complex Formation. A common method to estimate association constants, K_a, is to measure absorbance or initial PLI amplitude changes in titration experiments with the photocatalyst. These approaches are attractive because the K_a values are determined directly from experimental data, but report specifically on the ground-state association. While in some cases this may be a good approximation for the excited state, previous research has indicated substantially different ground-state and excited-state equilibria for polypyridyl complexes with halides.[57] Moreover, in the quenching titrations reported herein, negligible absorbance or photoluminescence amplitude changes were observed in all solvents except CH_2Cl_2 thereby precluding this approach (Figure S3-S10).

We therefore instead chose to use a theoretical model to estimate the association constant between the excited-state photocatalysts and halides that was applicable to the full series of solvents studied. The Fuoss expression given in Equation 24 was used to estimate K_a values, which

are tabulated in Table 5. In this expression, the work term, G_w, is the potential energy, $U(r)$, evaluated at the sum of the reactants' Van der Waals radii ($r = R$, Equation 25) and all other terms have been previously defined.

$$K_a = 1000\left(\frac{4}{3}\right)\pi R^3 N_A exp\left(\frac{-G_w}{k_b T}\right) \quad (24)$$

$$G_w = U(r=R) = \frac{z_a z_b e^2}{4\pi\varepsilon_r\varepsilon_0 r}\left(\frac{1}{2}\left(\frac{exp(\kappa\sigma_a)}{1+\kappa\sigma_a} + \frac{exp(\kappa\sigma_b)}{1+\kappa\sigma_b}\right)exp(-\kappa r)\right) \quad (25)$$

Scheme 2. Additional photocatalysts with different overall charge

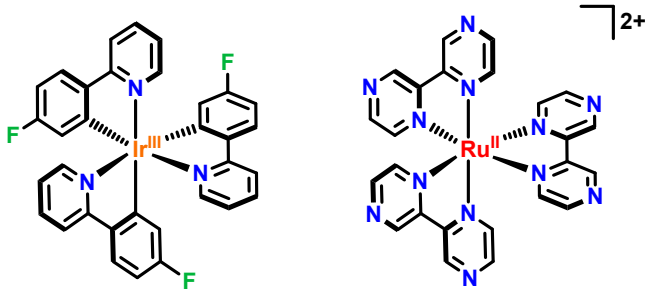

Ir(F-ppy)$_3$
$E^o(Ir^{+*/0})$ = 0.73 V

Ru(bpz)$_3^{2+}$
$E^o(Ru^{2+*/+})$ = 1.16 V

To probe the validity of the Fuoss expression for estimating K_a, Stern-Volmer titrations were performed with two additional photocatalysts (Scheme 2) in acetonitrile (Figure S16 and S17). Comparative studies with [Ir(F-ppy)$_3$] and [Ru(bpz)$_3$]$^{2+}$ provided insights into how the photocatalyst charge, +2,+1, and 0, impacted the extracted potential (Table 6). Of note, Ir(F-ppy)$_3$ is a weaker photooxidant that only provided sufficient driving force for iodide oxidation.[58] In addition, [Ru(bpz)$_3$]$^{2+}$ is known to undergo ligand-loss chemistry upon illumination in the presence of chloride and bromide; thus only quenching data with iodide is reported herein.[34,35,59] The limited scope of photocatalyst excited states that are quenched by all three halides without deleterious reactivity underscores the novelty of the photocatalysts chosen and their use for estimating halogen reduction potentials through semiclassical Marcus theory.

A review of the data in Table 6 shows that the K_a values for [Ir(F-ppy)$_3$]and [Ru(bpz)$_3$]$^{2+}$ calculated with the Fuoss equation with iodide were about a factor of 5 lower and higher, respectively, than those calculated for the parent Ir photocatalysts. With these K_a values, $E°'(I^{\bullet/-})$ were determined to be 0.70 V vs $Fc^{+/0}$ for [Ir(F-ppy)$_3$] and 0.66 V vs $Fc^{+/0}$ for [Ru(bpz)$_3$]$^{2+}$. Had the K_a values for the parent photocatalysts been used instead, the extracted $E°'(I^{\bullet/-})$ would have spanned a range of 0.43 – 0.78 V vs $Fc^{+/0}$. The ±0.04 V variance between photocatalysts with

substantially different K_a values suggests that the Fuoss expression provides a suitable estimate for encounter complex formation under these conditions.

Table 6. Association constants and formal reduction potentials determined with the indicated photocatalyst in CH_3CN.

Solvent	K_a I (M^{-1})[a]	$E°'(I^{\bullet/-})$[b]
Ir-4,4'-CF_3^+	8.95	0.69
Ir-5,5'-CF_3^+	8.95	0.67
[Ir(F-ppy)$_3$]	1.75	0.70
[Ru(bpz)$_3$]$^{2+}$	49.7	0.66

[a]Values were obtained from Equation 24 and 25 using a photocatalyst radius of 6.8 Å. [b]V vs $Fc^{+/0}$.

(6) Marcus Theory for Electron Transfer. The rate constant for electron transfer, k_{et}, reports on the free energy change for halide oxidation as described by Marcus theory (Equation 4) provided that the frequency factor, A, and the reorganization energy, λ, are known. For this study, a typical value of λ = 1 eV was assumed that arises from the outer-sphere solvent contributions and is consistent with negligibly small inner-sphere contributions[60] from the halogen $X^{\bullet/-}$ and the $Ir^{+*/0}$.[61–67] While dielectric continuum theory has been routinely employed to estimate λ in electron transfer reactions, the small size of un-solvated halides give rise to unrealistically large reorganization energies. Fortunately, halides display intense charge-transfer-to-solvent absorption bands in the ultraviolet region whose full width at half-maximum report on λ.[68] Previous analysis of these charge-transfer bands have indicated that λ differs by only 0.04 eV between iodide and chloride in water.[69] Reorganization energies are therefore expected to be near halide-independent, although some variance in λ across solvents is likely, which would change the absolute position of the halogen reduction potentials between solvents. Increasing λ to 1.2 eV resulted in $E°'(X^{\bullet/-})$ values that were decreased by 140 mV, whereas decreasing λ to 0.8 eV resulted in about a 140 mV increase in $E°'(X^{\bullet/-})$ (Figure S18).

The pre-exponential factor, A—which contains the electronic coupling matrix element, $|H_{AB}|^2$ (Equation 4)—was assumed to be 1.0 x10^{11} s^{-1}.[37,46,70] An order of magnitude change in A resulted in about an 180 mV shift to $E°'(X^{\bullet/-})$ (Figure S19). The relatively small range of $E°'(X^{\bullet/-})$ potentials extracted for the halogens in nonpolar solvents may suggest that coupling between the photocatalyst and the halide ion within the encounter complex is halide dependent.[71] This point is elaborated upon in Section 9.

(7) Excited State Reduction Potentials and Work Term. Within the Rehm-Weller expression (Equation 5), the excited-state reduction potential of the photocatalyst, $E°'(Ir^{*+/0})$, and work term, G_w, for associating the photocatalyst and halide are necessary to extract $E°'(X^{\bullet/-})$ from the $-\Delta G^o$ determined through Marcus theory. Excited-state reduction potentials were estimated using the ground state reduction potential and the free energy stored in the excited state, ΔG_{es}.[32,33] Franck-Condon line shape analysis of photoluminescence recorded at 77K have been used to precisely determine ΔG_{es}, but such measurements are limited to solvents that form a frozen glass and the rigid glass results in a significant blue shift. We therefore chose to use the more generalizable method of extrapolating a tangent line on the blue edge of the corrected PL spectrum to the emission baseline to estimate ΔG_{es}.[72,73]

The G_w used in the Rehm-Weller equation is identical to that used for K_a, once converted from SI units to eV (Equation 25). While the work term is routinely ignored in aqueous experiments, it is significant in nonpolar solvents especially at low ionic strengths. To test the impact of the work terms on this analysis, Stern-Volmer measurements were performed with Ir-4,4'-CF_3 and chloride in dichloromethane at 0.0, 0.005, and 0.1 M $TBAPF_6$. Table 7 reveals that the work term was –167 meV without the external electrolyte and was attenuated to –117 meV and –51 meV at 0.005 M and 0.1 M ionic strengths, respectively. Remarkably good agreement was found in the work term corrected halogen reduction potentials at all three ionic strengths provided in Table 7. This demonstrates both the importance of the work term for electron transfers in nonpolar solvents and the ability of Equation 25 to account for ionic interactions at various electrolyte concentrations in the estimation of $E°'(Cl^{\bullet/-})$.

Table 7. Work term (G_w), driving force for electron transfer ($-\Delta G^o$), and $E°'(Cl^{\bullet/-})$ values extracted from quenching measurements in dichloromethane.

	G_w[a] (meV)	$-\Delta G^o$[b] (eV)	$E°'(Cl^{\bullet/-})$[c] (V vs $Fc^{+/0}$)
No Electrolyte	–167	0.0634	1.04
0.005 M	–117	0.130	1.02
0.1 M	–51	0.198	1.02

[a]Values determined from Equation 25. [b]Values extracted from Equation 4 using $A = 10^{11}$ s^{-1} and $\lambda = 1$ eV. [c]Values estimated with Equation 5.

(8) Sensitivity Analysis to Estimate Uncertainty. A sensitivity analysis was performed to estimate the uncertainty in the extracted reduction potentials given in Table 3 resulting from

approximations for k_{diff}, K_a, λ, and A. The reorganization energy was varied from $\lambda = 0.5$ to 1.5 eV, the Marcus pre-exponential factor was varied from $A = 10^{10}$ to 10^{12} s^{-1}, the encounter complex association constants (K_a) were varied an order of magnitude smaller or larger than the values determined from the Fuoss equation (Equation 24), and the bimolecular diffusional rate constants (k_{diff}) were varied 25% from the value determined from Equation 14. The sensitivity to each parameter for $E°'(Cl^{\bullet/-})$, $E°'(Br^{\bullet/-})$, and $E°'(I^{\bullet/-})$ in acetonitrile is illustrated in Figure S20. The uncertainties given in Table 3 reflect the greatest deviation observed in the extracted reduction potentials from variation of the aforementioned parameters. In every case, the greatest deviation occurred when the reorganization energy was changed from $\lambda = 1$ eV to $\lambda = 0.5$ eV.

The sensitivity analysis revealed that the estimated reduction potentials for each halide and solvent are the same within uncertainty. This highlights the importance of sound assumptions for parameters whose values are unknown. Accordingly, a particularly large range for λ and A were evaluated in the sensitivity analysis since direct experimental measure of these values are absent in the literature for organic solvents. On the other hand, the assumptions of $\lambda = 1$ eV and $A = 10^{11}$ s^{-1} in water are supported by prior studies[46,61–67,70] where reorganization energies have been shown to be invariant with halide identity[69] and there is no evidence for strong coupling between halides and photocatalysts. Nonpolar solvents such as dichloromethane are likely to lead to stronger halide-photocatalyst coupling where solvation of charged species is poorly understood. Consequently, deviations from commonly assumed parameters are more likely and the uncertainty in $E°'(X^{\bullet/-})$ needs to be considered within this context.

(9) Evaluation of Estimated Halogen Reduction Potentials. The $E°'(X^{\bullet/-})$ values determined kinetically are gathered in Table 3 and are evaluated here versus a common NHE reference (note that the nonaqueous potentials in Table 3 are reported vs $Fc^{+/0}$, which is shifted by 0.623 V vs NHE in CH_3CN[74]). A previously reported $E°'(I^{\bullet/-}) = 1.23$ V vs NHE in CH_3CN from stopped flow kinetic experiments[22] is in fair agreement with the data reported herein of 1.30 V vs NHE. The kinetic data in water revealed $E°'(I^{\bullet/-}) = 1.27$ V vs NHE and $E°'(Br^{\bullet/-}) = 1.84$ V vs NHE that are in reasonable agreement with values from pulse radiolysis studies of 1.33 and 1.92 V vs NHE for iodide and bromide, respectively.[16] No experimental evidence for chloride oxidation in water was evident with these photocatalysts. This is unfortunate as an unusually large range of aqueous $E°'(Cl^{\bullet/-})$ = 2.2 to 2.4 V vs NHE have been reported in the literature.[9,16] Previously reported force field calculations reveal that 20% of the chloride electron density is transferred to

the coordinated water through H-bonds.[75–77] Indeed, there is growing evidence for H-bonding of organic solvents to halides as revealed by x-ray crystallography[78–82] and ^{1}H NMR experiments.[83] Charge delocalization to solvent would result in a more positive $E°'(Cl^{\bullet/-})$ in water relative to those in weaker H-bonding solvents when the same number of interactions are present. This report of chloride quenching in propylene carbonate, acetonitrile, butyronitrile, and dichloromethane affirms that the $E°'(Cl^{\bullet/-})$ are significantly more thermodynamically favorable in organic solvents than water.

It is noteworthy that the expected periodic trend, $E°'(I^{\bullet/-}) < E°'(Br^{\bullet/-}) < E°'(Cl^{\bullet/-})$, is evident in each solvent.[9] However, there is a relatively small positive shift in $E°'(X^{\bullet/-})$ as one proceeds toward the more electronegative halogens in organic solvents. The difference between $E°'(I^{\bullet/-})$ and $E°'(Cl^{\bullet/-})$ range from 210 mV in propylene carbonate to 40 mV in dichloromethane, which trend with the decrease in solvent dielectric constant. This is in stark contrast to water where an ~ 1 V separation has been reported.[9,16,17] Likewise, the gas phase electron affinities span 0.55 eV from I (3.06 eV),[84] Br (3.36 eV),[85] and Cl (3.61 eV),[86] with an interesting reversal for F (3.40 eV).[85]

The similarity of $E°'(X^{\bullet/-})$ between halogen congeners in nonpolar solvents is surprising and suggests that perhaps one or more of the underlying assumptions may be invalid. Previous ^{1}H NMR studies of halide ion pairing with ruthenium polypyridyl photocatalysts have provided direct evidence for adduct formation with the most acidic 3 and 3' H atoms of the bipyridine ligands[87] with measurable affinity differences between iodide, bromide, and chloride.[29] The presence of ethyl ester functional groups in the 4 and 4' positions inhibited this interaction, while quaternary amine substituents enhanced ion pairing.[29,59,88–90] This prior ion-pairing data suggests that electronic coupling pathways through aromatic ligands may result in halide-specific coupling and hence A values that can be tuned by the incorporation of specific functional groups. Another consideration is halogen atom stabilization by aromatic ligands. Halogen-π complexes are well known and have been spectroscopically quantified.[12,13,99–101,91–98] Computational studies indicate that the interaction of a halogen atom with benzene resulted in a stabilization of up to 225 meV for chloride and less than 90 meV for iodide.[102] Taken together, these previous halide ion-pairing and halogen atom reports suggest that alternative 'inner-sphere' mechanistic pathways for halide oxidation may be accessed under some experimental conditions. The impact of such a putative inner-sphere pathway on electronic coupling and free energy is of great interest and provides new opportunities for future research.

CONCLUSION

In conclusion, visible light generated excited states of $(d\pi)^6$ inorganic photocatalysts were quenched by halides in propylene carbonate, acetonitrile, butyronitrile, dichloromethane, and water. The quenching mechanism was attributed to dynamic electron transfer, and Stern-Volmer analysis was performed to extract kinetic information that reported on halogen-atom formation. This kinetic data was used to estimate the one-electron halogen reduction potentials that are inaccessible through traditional electrochemistry. Determination of $E°'(X^{\bullet/-})$ necessitated a number of approximations and assumptions, which warranted individual evaluation. A diffusional model was used to relate the observed quenching rate constant to the electron transfer rate constant, which required knowledge of diffusion and encounter complex association. Estimations of bimolecular diffusional rate constants of ionic species are difficult, particularly in low dielectric solvents and/or high ionic strengths. However, it was shown that diffusion of charged species can be adequately determined even in relatively nonpolar solvents such as dichloromethane when an appropriately sophisticated model is used. Photocatalysts with a 0, 1+, and 2+ charge had markedly different association constants with iodide, yet yielded self-consistent $E°'(I^{\bullet/-})$ values.

A sensitivity analysis was performed on the reported $E°'(X^{\bullet/-})$ values where large, yet physically reasonable, bounds were used for the k_{diff}, K_a, λ, and A. This analysis revealed that the estimated potentials were the same within the uncertainty of the model. However, when parameters commonly used in aqueous solutions were utilized, the extracted aqueous $E°'(X^{\bullet/-})$ values for X = Br and I were in remarkable agreement with the literature indicating that the kinetic approach is fundamentally sound. Uncertainty in the estimated values of $E°'(X^{\bullet/-})$ most likely emanate from assumptions within the Marcus analysis. The assumptions that λ and A are invariant with solvent and halide may lead to systematic errors in $E°'(X^{\bullet/-})$; we therefore advise caution when considering the values reported herein. The remarkably small separation between halides in less polar solvents is indeed curious. Whether this is a real effect or perhaps due to enhanced electronic coupling with smaller halides, a stabilizing interaction of the photocatalyst with the halogen atom, or another yet-to-be-identified contributor is not known and warrants future study. It seems prudent to note that this is the *only* study to report and compare experimentally determined $E°'(X^{\bullet/-})$ values in organic solvents. We therefore hope others will continue to critically examine and refine these estimates to further our understanding of fundamental properties of halogen atoms in organic solutions.

ASSOCIATED CONTENT

Supporting Information. Electron transfer rate constants, solvent parameters, time-resolved photoluminescence quenching, Stern-Volmer plots, and transient absorption spectroscopy. The Supporting Information is available free of charge on the ACS Publications website.

AUTHOR INFORMATION

Corresponding Author

gjmeyer@email.unc.edu

Present Addresses

⊥Laboratoire de Chimie Organique, Université Libre de Bruxelles (ULB), CP 160/06, 50 avenue F.D. Roosevelt, B-1050 Brussels, Belgium.

Author Contributions

The manuscript was written through contributions of all authors. All authors have given approval to the final version of the manuscript.

Notes

The authors declare no competing financial interests.

ACKNOWLEDGMENT

The research was supported by the National Science Foundation under Award CHE-1465060. L.T.-G. acknowledges the F.R.S.-FNRS for an individual "Chargé de Recherches" fellowship. The authors acknowledge Carla M. Morton and Erik J. Alexanian for the gift of Ir-5,5'-CF_3.

REFERENCES

(1) Brady, M. D.; Sampaio, R. N.; Wang, D.; Meyer, T. J.; Meyer, G. J. Dye-Sensitized Hydrobromic Acid Splitting for Hydrogen Solar Fuel Production. *J. Am. Chem. Soc.* **2017**, *139* (44), 15612–15615.

(2) Brady, M. D.; Troian-Gautier, L.; Sampaio, R. N.; Motley, T. C.; Meyer, G. J. Optimization of Photocatalyst Excited- and Ground-State Reduction Potentials for Dye-Sensitized HBr Splitting. *ACS Appl. Mater. Interfaces* **2018**, *10* (37), 31312–31323.

(3) McDaniel, N. D.; Bernhard, S. Solar Fuels: Thermodynamics, Candidates, Tactics, and Figures of Merit. *Dalt. Trans.* **2010**, *39* (42), 10021–10030.

(4) Mei, B.; Mul, G.; Seger, B. Beyond Water Splitting: Efficiencies of Photo-Electrochemical Devices Producing Hydrogen and Valuable Oxidation Products. *Adv. Sustain. Syst.* **2017**, *1*, 1600035.

(5) Nocera, D. G. Chemistry of Personalized Solar Energy. *Inorg. Chem.* **2009**, *48* (21), 10001–10017.

(6) Ardo, S.; Park, S. H.; Warren, E. L.; Lewis, N. S. Unassisted Solar-Driven Photoelectrosynthetic HI Splitting Using Membrane-Embedded Si Microwire Arrays. *Energy Environ. Sci.* **2015**, *8* (5), 1484–1492.

(7) Rohe, S.; Morris, A. O.; McCallum, T.; Barriault, L. Hydrogen Atom Transfer Reactions via Photoredox Catalyzed Chlorine Atom Generation. *Angew. Chem. Int. Ed.* **2018**, *57* (48), 15664–15669.

(8) Twilton, J.; Le, C. C.; Zhang, P.; Shaw, M. H.; Evans, R. W.; MacMillan, D. W. C. The Merger of Transition Metal and Photocatalysis. *Nat. Rev. Chem.* **2017**, *1*.

(9) Troian-Gautier, L.; Turlington, M. D.; Wehlin, S. A. M.; Maurer, A. B.; Brady, M. D.; Swords, W. B.; Meyer, G. J. Halide Photoredox Chemistry. *Chem. Rev.* **2019**, *119* (7), 4628–4683.

(10) Yang, Q.; Wang, Y. H.; Qiao, Y.; Gau, M.; Carroll, P. J.; Walsh, P. J.; Schelter, E. J. Photocatalytic C-H Activation and the Subtle Role of Chlorine Radical Complexation in Reactivity. *Science* **2021**, *372* (6544), 847–852.

(11) Shields, B. J.; Doyle, A. G. Direct C(Sp3)-H Cross Coupling Enabled by Catalytic Generation of Chlorine Radicals. *J. Am. Chem. Soc.* **2016**, *138* (39), 12719–12722.

(12) Hwang, S. J.; Powers, D. C.; Maher, A. G.; Anderson, B. L.; Hadt, R. G.; Zheng, S.-L.;

Chen, Y.-S.; Nocera, D. G. Trap-Free Halogen Photoelimination from Mononuclear Ni(III) Complexes. *J. Am. Chem. Soc.* **2015**, *137* (20), 6472–6475.

(13) Hwang, S. J.; Anderson, B. L.; Powers, D. C.; Maher, A. G.; Hadt, R. G.; Nocera, D. G. Halogen Photoelimination from Monomeric Nickel(III) Complexes Enabled by the Secondary Coordination Sphere. *Organometallics* **2015**, *34* (19), 4766–4774.

(14) Bentley, C. L.; Bond, A. M.; Hollenkamp, A. F.; Mahon, P. J.; Zhang, J. Voltammetric Determination of the Iodide/Iodine Formal Potential and Triiodide Stability Constant in Conventional and Ionic Liquid Media. *J. Phys. Chem. C* **2015**, *119* (39), 22392–22403.

(15) Isse, A. A.; Lin, C. Y.; Coote, M. L.; Gennaro, A. Estimation of Standard Reduction Potentials of Halogen Atoms and Alkyl Halides. *J. Phys. Chem. B* **2011**, *115* (4), 678–684.

(16) Stanbury, D. M. REDUCTION POTENTIALS INVOLVING INORGANIC FREE RADICALS IN AQUEOUS SOLUTION. *Adv. Inorg. Chem.* **1989**, *33*, 11–111.

(17) Schwarz, H. A.; Dodson, R. W. Equilibrium between Hydroxyl Radicals and Thallium(II) and the Oxidation Potential of Hydroxyl(Aq). *J. Phys. Chem.* **1984**, *88* (16), 3643–3647.

(18) Schwarz, H. A.; Bielski, B. H. J. Reactions of HO2 and O2- with Iodine and Bromine and the I2- and I Atom Reduction Potentials. *J. Phys. Chem.* **1986**, *90* (7), 1445–1448.

(19) Wardman, P. Reduction Potentials of One-Electron Couples Involving Free Radicals in Aqueous Solution. *J. Phys. Chem. Ref. Data* **1989**, *18* (4), 1637–1755.

(20) Armstrong, D. A.; Huie, R. E.; Lymar, S.; Koppenol, W. H.; Merényi, G.; Neta, P.; Stanbury, D. M.; Steenken, S.; Wardman, P. Standard Electrode Potentials Involving Radicals in Aqueous Solution: Inorganic Radicals. *Bioinorg. React. Mech.* **2013**, *9* (1–4), 59–61.

(21) Piechota, E. J.; Meyer, G. J. Introduction to Electron Transfer: Theoretical Foundations and Pedagogical Examples. *J. Chem. Educ.* **2019**, *96* (11), 2450–2466.

(22) Wang, X.; Stanbury, D. M. Oxidation of Iodide by a Series of Fe(III) Complexes in Acetonitrile. *Inorg. Chem.* **2006**, *45* (8), 3415–3423.

(23) Newton, M. D.; Sutin, N. Electron Transfer Reactions in Condensed Phases. *Annu. Rev. Phys. Chem.* **1984**, *35* (1), 437–480.

(24) Chiorboli, C.; Indelli, M. T.; Scandola, M. A. R.; Scandola, F. Salt Effects on Nearly Diffusion Controlled Electron-Transfer Reactions. Bimolecular Rate Constants and Cage

Escape Yields in Oxidative Quenching of Tris(2,2′-Bipyridine)Ruthenium(II). *J. Phys. Chem.* **1988**, *92* (1), 156–163.

(25) Romero, N. A.; Nicewicz, D. A. Organic Photoredox Catalysis. *Chem. Rev.* **2016**, *116* (17), 10075–10166.

(26) Shaw, M. H.; Twilton, J.; MacMillan, D. W. C. Photoredox Catalysis in Organic Chemistry. *J. Org. Chem.* **2016**, *81* (16), 6898–6926.

(27) Wang, C.-S.; Dixneuf, P. H.; Soulé, J.-F. Photoredox Catalysis for Building C–C Bonds from C(Sp 2)–H Bonds. *Chem. Rev.* **2018**, *118* (16), 7532–7585.

(28) Argazzi, R.; Bignozzi, C. A.; Heimer, T. A.; Castellano, F. N.; Meyer, G. J. Enhanced Spectral Sensitivity from Ruthenium(II) Polypyridyl Based Photovoltaic Devices. *Inorg. Chem.* **1994**, *33* (25), 5741–5749.

(29) Troian-Gautier, L.; Beauvilliers, E. E.; Swords, W. B.; Meyer, G. J. Redox Active Ion-Paired Excited States Undergo Dynamic Electron Transfer. *J. Am. Chem. Soc.* **2016**, *138* (51), 16815–16826.

(30) DiMarco, B. N.; Troian-Gautier, L.; Sampaio, R. N.; Meyer, G. J. Dye-Sensitized Electron Transfer from TiO 2 to Oxidized Triphenylamines That Follows First-Order Kinetics. *Chem. Sci.* **2018**, *9* (4), 940–949.

(31) Deaton, J. C.; Castellano, F. N. Archetypal Iridium(III) Compounds for Optoelectronic and Photonic Applications. In *Iridium(III) in Optoelectronic and Photonics Applications*; 2017; pp 1–69.

(32) Thompson, D. W.; Ito, A.; Meyer, T. J. [Ru(Bpy)3]2+* and Other Remarkable Metal-to-Ligand Charge Transfer (MLCT) Excited States*. *Pure Appl. Chem.* **2013**, *85* (7), 1257–1305.

(33) Adamson, A. W.; Namnath, J.; Shastry, V. J.; Slawson, V. Thermodynamic Inefficiency of Conversion of Solar Energy to Work. *J. Chem. Educ.* **1984**, *61* (3), 221–224.

(34) Li, G.; Brady, M. D.; Meyer, G. J. Visible Light Driven Bromide Oxidation and Ligand Substitution Photochemistry of a Ru Diimine Complex. *J. Am. Chem. Soc.* **2018**, *140* (16), 5447–5456.

(35) Luis, E. T.; Iranmanesh, H.; Beves, J. E. Photosubstitution Reactions in Ruthenium(II) Trisdiimine Complexes: Implications for Photoredox Catalysis. *Polyhedron* **2019**, *160*, 1–9.

(36) White, J. K.; Schmehl, R. H.; Turro, C. An Overview of Photosubstitution Reactions of Ru(II) Imine Complexes and Their Application in Photobiology and Photodynamic Therapy. *Inorg. Chim. Acta* **2017**, *454*, 7–20.

(37) Bevernaegie, R.; Wehlin, S. A. M.; Piechota, E. J.; Abraham, M.; Philouze, C.; Meyer, G. J.; Elias, B.; Troian-Gautier, L. Improved Visible Light Absorption of Potent Iridium(III) Photo-Oxidants for Excited-State Electron Transfer Chemistry. *J. Am. Chem. Soc.* **2020**, *142* (6), 2732–2737.

(38) Gardner, J. M.; Abrahamsson, M.; Farnum, B. H.; Meyer, G. J. Visible Light Generation of Iodine Atoms and I-I Bonds: Sensitized I - Oxidation and I3- Photodissociation. *J. Am. Chem. Soc.* **2009**, *131* (44), 16206–16214.

(39) Rehm, D.; Weller, A. Kinetics of Fluorescence Quenching by Electron and H-Atom Transfer. *Isr. J. Chem.* **1970**, *8* (2), 259–271.

(40) Rehm, D.; Weller, A. Kinetik Und Mechanismus Der Elektronübertragung Bei Der Fluoreszenzlöschung in Acetonitril. *Berichte der Bunsengesellschaft für Phys. Chemie* **1969**, *73* (8-9), 834–839.

(41) Steinfeld, J. I.; Francisco, J. S.; Hase, W. L. *Chemical Kinetics and Dynamics*, 2nd ed.; Prentice Hall: Upper Saddle River, New Jersey, 1999.

(42) Shannon, R. D. Revised Effective Ionic Radii and Systematic Studies of Interatomic Distances in Halides and Chalcogenides. *Acta Crystallogr. Sect. A* **1976**, *32* (5), 751–767.

(43) Braslavsky, S. E. Glossary of Terms Used in Photochemistry, 3rd Edition (IUPAC Recommendations 2006). *Pure Appl. Chem.* **2007**, *79* (3), 293–465.

(44) Fuoss, R. M. Ionic Association. III. The Equilibrium between Ion Pairs and Free Ions. *J. Am. Chem. Soc.* **1958**, *80* (19), 5059–5061.

(45) Brown, G. M.; Sutin, N. A Comparison of the Rates of Electron Exchange Reactions of Ammine Complexes of Ruthenium(II) and-(III) with the Predictions of Adiabatic, Outer-Sphere Electron Transfer Models. *J. Am. Chem. Soc.* **1979**, *101* (4), 883–892.

(46) Sutin, N. Nuclear, Electronic, and Frequency Factors in Electron-Transfer Reactions. *Acc. Chem. Res.* **1982**, *15* (9), 275–282.

(47) Debye, P. Reaction Rates in Ionic Solutions. *Trans. Electrochem. Soc.* **1942**, *82* (1), 265.

(48) Marcus, R. A.; Siders, P. Theory of Highly Exothermic Electron Transfer Reactions. *J. Phys. Chem.* **1982**, *86* (5), 622–630.

(49) Elliot, A. J.; McCracken, D. R.; Buxton, G. V.; Wood, N. D. Estimation of Rate Constants for Near-Diffusion-Controlled Reactions in Water at High Temperatures. *J. Chem. Soc. Faraday Trans.* **1990**, *86* (9), 1539–1547.

(50) Krise, K. M.; Hwang, A. A.; Milosavljevic, B. H. Analysis and Improvement of Rate Constant Determination of Reactions Involving Charged Reactants. *Phys. Chem. Chem. Phys.* **2010**, *12* (27), 7695–7701.

(51) Weston, R. E.; Schwarz, H. A. *Chemical Kinetics*; Prentice Hall: Englewood Cliffs, NJ, 1972.

(52) Farnum, B. H.; Gardner, J. M.; Meyer, G. J. Flash-Quench Technique Employed to Study the One-Electron Reduction of Triiodide in Acetonitrile: Evidence for a Diiodide Reaction Product. *Inorg. Chem.* **2010**, *49* (22), 10223–10225.

(53) Chiorboli, C.; Scandola, F.; Kisch, H. Quenching of Excited Tris(2,2′-Bipyridine)Ruthenium(II) by Metal 1,2-Dithiolene Complexes. *J. Phys. Chem.* **1986**, *90* (10), 2211–2215.

(54) Bao, D.; Millare, B.; Xia, W.; Steyer, B. G.; Gerasimenko, A. A.; Ferreira, A.; Contreras, A.; Vullev, V. I. Electrochemical Oxidation of Ferrocene: A Strong Dependence on the Concentration of the Supporting Electrolyte for Nonpolar Solvents. *J. Phys. Chem. A* **2009**, *113* (7), 1259–1267.

(55) Bird, M. J.; Pearson, M. A.; Asaoka, S.; Miller, J. R. General Method for Determining Redox Potentials without Electrolyte. *J. Phys. Chem. A* **2020**, *124* (26), 5487–5495.

(56) Deng, H. P.; Zhou, Q.; Wu, J. Microtubing-Reactor-Assisted Aliphatic C−H Functionalization with HCl as a Hydrogen-Atom-Transfer Catalyst Precursor in Conjunction with an Organic Photoredox Catalyst. *Angew. Chemie - Int. Ed.* **2018**, *57* (39), 12661–12665.

(57) Turlington, M. D.; Troian-Gautier, L.; Sampaio, R. N.; Beauvilliers, E. E.; Meyer, G. J. Control of Excited-State Supramolecular Assembly Leading to Halide Photorelease. *Inorg. Chem.* **2019**, *58* (5), 3316–3328.

(58) Singh, A.; Teegardin, K.; Kelly, M.; Prasad, K. S.; Krishnan, S.; Weaver, J. D. Facile Synthesis and Complete Characterization of Homoleptic and Heteroleptic Cyclometalated Iridium(III) Complexes for Photocatalysis. *J. Organomet. Chem.* **2015**, *776*, 51–59.

(59) Wehlin, S. A. M. M.; Troian-Gautier, L.; Li, G.; Meyer, G. J. Chloride Oxidation by

Ruthenium Excited-States in Solution. *J. Am. Chem. Soc.* **2017**, *139* (37), 12903–12906.

(60) Biner, M.; Buergi, H. B.; Ludi, A.; Roehr, C. Crystal and Molecular Structures of [Ru(Bpy)3](PF6)3 and [Ru(Bpy)3](PF6)2 at 105 K. *J. Am. Chem. Soc.* **1992**, *114* (13), 5197–5203.

(61) Brunschwig, B. S.; Creutz, C.; Sutin, N.; Cambridge, R.; January, U. K. Optical Transitions of Symmetrical Mixed-Valence Systems in the Class II–III Transition Regime. *Chem. Soc. Rev.* **2002**, *31* (3), 168–184.

(62) Fox, L. S.; Kozik, M.; Winkler, J. R.; Gray, H. B. Gaussian Free-Energy Dependence of Electron-Transfer Rates in Iridium Complexes. *Science* **1990**, *247* (4946), 1069–1071.

(63) Gust, D.; Moore, T. A.; Moore, A. L. Molecular Mimicry of Photosynthetic Energy and Electron Transfer. *Acc. Chem. Res.* **1993**, *26* (4), 198–205.

(64) Yonemoto, E. H.; Saupe, G. B.; Riley, R. L.; Iverson, B. L.; Schmehl, R. H.; Hubig, S. M.; Mallouk, T. E. Electron-Transfer Reactions of Ruthenium Trisbipyridyl-Viologen Donor-Acceptor Molecules: Comparison of the Distance Dependence of Electron-Transfer Rates in the Normal and Marcus Inverted Regions. *J. Am. Chem. Soc.* **1994**, *116* (11), 4786–4795.

(65) Yonemoto, E. H.; Riley, R. L.; Kim, Y. Il; Atherton, S. J.; Schmehl, R. H.; Mallouk, T. E. Photoinduced Electron Transfer in Covalently Linked Ruthenium Tris(Bipyridyl)-Viologen Molecules: Observation of Back Electron Transfer in the Marcus Inverted Region. *J. Am. Chem. Soc.* **1992**, *114* (21), 8081–8087.

(66) Gennett, T.; Milner, D. F.; Weaver, M. J. Role of Solvent Reorganization Dynamics in Electron-Transfer Processes. Theory-Experiment Comparisons for Electrochemical and Homogeneous Electron Exchange Involving Metallocene Redox Couples. *J. Phys. Chem.* **1985**, *89* (13), 2787–2794.

(67) Lopez-Lopez, M.; Sanchez, F.; Marchena, M. Determination of Reaction and Reorganization Free Energies of Electron Transfer Reactions under Restricted Geometry Conditions. *Prog. React. Kinet. Mech.* **2012**, *37* (3), 203–248.

(68) Piechota, E. J.; Troian-Gautier, L.; Sampaio, R. N.; Brennaman, M. K.; Hu, K.; Berlinguette, C. P.; Meyer, G. J. Optical Intramolecular Electron Transfer in Opposite Directions through the Same Bridge That Follows Different Pathways. *J. Am. Chem. Soc.* **2018**, *140* (23), 7176–7186.

(69) Gorelsky, S. I.; Kotov, V. Y.; Lever, A. B. P. Vertical Ionization Energies and Electron Affinities of Ions in Solution from Outer-Sphere Charge Transfer Transition Energies. *Inorg. Chem.* **1998**, *37* (18), 4584–4588.

(70) Marcus, R. A. On the Frequency Factor in Electron Transfer Reactions and Its Role in the Highly Exothermic Regime. *Int. J. Chem. Kinet.* **1981**, *13* (9), 865–872.

(71) Sampaio, R. N.; Piechota, E. J.; Troian-Gautier, L.; Maurer, A. B.; Hu, K.; Schauer, P. A.; Blair, A. D.; Berlinguette, C. P.; Meyer, G. J. Kinetics Teach That Electronic Coupling Lowers the Free-Energy Change That Accompanies Electron Transfer. *Proc. Natl. Acad. Sci.* **2018**, *115* (28), 7248–7253.

(72) Yarnell, J. E.; McCusker, C. E.; Leeds, A. J.; Breaux, J. M.; Castellano, F. N. Exposing the Excited-State Equilibrium in an IrIII Bichromophore: A Combined Time Resolved Spectroscopy and Computational Study. *Eur. J. Inorg. Chem.* **2016**, *2016* (12), 1808–1818.

(73) McCusker, C. E.; Chakraborty, A.; Castellano, F. N. Excited State Equilibrium Induced Lifetime Extension in a Dinuclear Platinum(II) Complex. *J. Phys. Chem. A* **2014**, *118* (45), 10391–10399.

(74) Aranzaes, J. R.; Daniel, M. C.; Astruc, D. Metallocenes as References for the Determination of Redox Potentials by Cyclic Voltammetry - Permethylated Iron and Cobalt Sandwich Complexes, Inhibition by Polyamine Dendrimers, and the Role of Hydroxy-Containing Ferrocenes. *Can. J. Chem.* **2006**, *84* (2), 288–299.

(75) Liu, Y.; Sengupta, A.; Raghavachari, K.; Flood, A. H. Anion Binding in Solution: Beyond the Electrostatic Regime. *Chem* **2017**, *3* (3), 411–427.

(76) Cremer, P. S.; Flood, A. H.; Gibb, B. C.; Mobley, D. L. Collaborative Routes to Clarifying the Murky Waters of Aqueous Supramolecular Chemistry. *Nat. Chem.* **2018**, *10* (1), 8–16.

(77) Rogers, D. M.; Beck, T. L. Quasichemical and Structural Analysis of Polarizable Anion Hydration. *J. Chem. Phys.* **2010**, *132* (1), 014505.

(78) Li, A. Y. Theoretical Study of Linear and Bifurcated H-Bonds in the Systems Y···H2CZn (N=1, 2; Z = O, S, Se, F, Cl, Br; Y=Cl−, Br−). *J. Mol. Struct. THEOCHEM* **2008**, *862* (1–3), 21–27.

(79) Wu, Y.; Zhao, X.; Gao, H.; Jin, W. Triangular Halogen Bond and Hydrogen Bond

Supramolecular Complex Consisting of Carbon Tetrabromide, Halide, and Solvent Molecule: A Theoretical and Spectroscopic Study. *Chinese J. Chem. Phys.* **2014**, *27* (3), 265–273.

(80) Bait, S.; Chattel, G. du; Kieviet, W. de; Tieleman, A. Ion Association and Solvation in Dichloromethane of Tetrachloro-and Tetrabromoferrates(III) Compared with Simple Halides. *Zeitschrift für Naturforsch. B* **1978**, *33* (7), 745–749.

(81) Kryachko, E. S.; Zeegers-Huyskens, T. Theoretical Study of the CH···X - Interaction of Fluoromethanes and Chloromethanes with Fluoride, Chloride, and Hydroxide Anions. *J. Phys. Chem. A* **2002**, *106* (29), 6832–6838.

(82) Allen, F. H.; Wood, P. A.; Galek, P. T. A. Role of Chloroform and Dichloromethane Solvent Molecules in Crystal Packing: An Interaction Propensity Study. *Acta Crystallogr. Sect. B Struct. Sci. Cryst. Eng. Mater.* **2013**, *69* (4), 379–388.

(83) Assiri, Y.; Rahman, S.; Georghiou, P. E. Halide Ion Effect on the 1H NMR Chemical Shifts of the Residual Protons in Commonly Employed Deuterated Solvents with Tetra-n-Butylammonium Chloride – Part 2. *Supramol. Chem.* **2016**, *28* (1–2), 6–9.

(84) Pelez, R. J.; Blondel, C.; Delsart, C.; Drag, C. Pulsed Photodetachment Microscopy and the Electron Affinity of Iodine. *J. Phys. B At. Mol. Opt. Phys.* **2009**, *42* (12).

(85) Blondel, C.; Cacciani, P.; Delsart, C.; Trainham, R. High-Resolution Determination of the Electron Affinity of Fluorine and Bromine Using Crossed Ion and Laser Beams. *Phys. Rev. A* **1989**, *40* (7), 3698–3701.

(86) Berzinsh, U.; Gustafsson, M.; Hanstorp, D.; Klinkmüller, A.; Ljungblad, U.; Mårtensson-Pendrill, A.-M. Isotope Shift in the Electron Affinity of Chlorine. *Phys. Rev. A* **1995**, *51* (1), 231–238.

(87) Ward, W. M.; Farnum, B. H.; Siegler, M.; Meyer, G. J. Chloride Ion-Pairing with Ru(II) Polypyridyl Compounds in Dichloromethane. *J. Phys. Chem. A* **2013**, *117* (36), 8883–8894.

(88) Swords, W. B.; Li, G.; Meyer, G. J. Iodide Ion Pairing with Highly Charged Ruthenium Polypyridyl Cations in CH3CN. *Inorg. Chem.* **2015**, *54* (9), 4512–4519.

(89) Wehlin, S. A. M.; Troian-Gautier, L.; Sampaio, R. N.; Marcélis, L.; Meyer, G. J. Ter-Ionic Complex That Forms a Bond Upon Visible Light Absorption. *J. Am. Chem. Soc.* **2018**, *140* (25), 7799–7802.

(90) Troian-Gautier, L.; Wehlin, S. A. M.; Meyer, G. J. Photophysical Properties of Tetracationic Ruthenium Complexes and Their Ter-Ionic Assemblies with Chloride. *Inorg. Chem.* **2018**, *57* (19), 12232–12244.

(91) Walling, C. The Transient Species in Radical Chlorination in Benzene Solvent. *J. Org. Chem.* **1988**, *53* (2), 305–308.

(92) Raner, K. D.; Lusztyk, J.; Ingold, K. U. Kinetic Analysis of Alkane Polychlorination with Molecular Chlorine. Chlorine Atom/Monochloride Geminate Pairs and the Effect of Reactive Cage Walls on the Competition between Monochloride Rotation and Chlorine Atom Escape. *J. Am. Chem. Soc.* **1988**, *110* (11), 3519–3524.

(93) Raner, K. D.; Lusztyk, J.; Ingold, K. U. Ultraviolet/Visible Spectra of Halogen Molecule/Arene and Halogen Atom/Arene .Pi.-Molecular Complexes. *J. Phys. Chem.* **1989**, *93* (2), 564–570.

(94) Ingold, K. U.; Lusztyk, J.; Raner, K. D. The Unusual and the Unexpected in an Old Reaction. The Photochlorination of Alkanes with Molecular Chlorine in Solution. *Acc. Chem. Res.* **1990**, *23* (7), 219–225.

(95) Bunce, N. J.; Ingold, K. U.; Landers, J. P.; Lusztyk, J.; Scaiano, J. C. Kinetic Study of the Photochlorination of 2,3-Dimethylbutane and Other Alkanes in Solution in the Presence of Benzene. First Measurements of the Absolute Rate Constants for Hydrogen Abstraction by the "Free" Chlorine Atom and the Chlorine Atom-Benzene Pi. *J. Am. Chem. Soc.* **1985**, *107* (19), 5464–5472.

(96) McGimpsey, W. G.; Scaiano, J. C. Photochemistry of α-Chloro- and α-Bromoacetophenone. Determination of Extinction Coefficients for Halogen–Benzene Complexes. *Can. J. Chem.* **1988**, *66* (6), 1474–1478.

(97) Benson, S. W. Some Observations on the π-Complex of Cl Atoms with Benzene. *J. Am. Chem. Soc.* **1993**, *115* (15), 6969–6974.

(98) BÜHLER, R. E.; EBERT, M. Transient Charge-Transfer Complexes with Chlorine Atoms by Pulse Radiolysis of Carbon Tetrachloride Solutions. *Nature* **1967**, *214* (5094), 1220–1221.

(99) Strong, R. L.; Rand, S. J.; Britt, J. A. Charge-Transfer Spectra of Iodine Atom-Aromatic Hydrocarbon Complexes 1. *J. Am. Chem. Soc.* **1960**, *82* (19), 5053–5057.

(100) Förgeteg, S.; Bérces, T. Laser Flash Photolysis Study of Chlorine Atom/Simple Arene π-

Complexes in Carbon Tetrachloride and Acetonitrile. *J. Photochem. Photobiol. A Chem.* **1993**, *73* (3), 187–195.

(101) Bossy, J. M.; Buehler, R. E.; Ebert, M. Pulse Radiolysis of Organic Halogen Compounds. II. Transient Bromine-Atom Charge-Transfer Complexes Observed by Pulse Radiolysis. *J. Am. Chem. Soc.* **1970**, *92* (4), 1099–1101.

(102) Tsao, M. L.; Hadad, C. M.; Platz, M. S. Computational Study of the Halogen Atom-Benzene Complexes. *J. Am. Chem. Soc.* **2003**, *125* (27), 8390–8399.

“TOC Graphic”